
Article:
Bagheri, F., Biricik, S. orcid.org/0000-0002-1559-2024, Ahmed, H. orcid.org/0000-0001-8952-4190 et al. (1 more author) (2024) A second-order sliding mode control with active disturbance rejection for dynamic voltage restorers. IET Power Electronics, 17 (9). pp. 1133-1144. ISSN 1755-4535

https://doi.org/10.1049/pel2.12490

Received: 19 January 2023 | Revised: 25 February 2023 | Accepted: 14 March 2023

IET Power Electronics

DOI: 10.1049/pel2.12490

The Institution of Engineering and Technology WILEY

ORIGINAL RESEARCH

A second-order sliding mode control with active disturbance rejection for dynamic voltage restorers

Farzaneh Bagheri[1] | Samet Biricik[2] | Hafiz Ahmed[3] | Hasan Komurcugil[4]

[1]Department of Electrical and Electronic Engineering, Antalya Bilim University, Antalya, Turkey

[2]Department of Electrical and Electronic Engineering, European University of Lefke, Lefke Mersin 10, Turkey

[3]Nuclear Futures Institute, Bangor University, Bangor, UK

[4]Department of Computer Engineering, Eastern Mediterranean University, Famagusta Mersin 10, Turkey

Correspondence
Hafiz Ahmed, Dean Street, Bangor LL57 2DG, Gwynedd, UK.
Email: hafiz.h.ahmed@ieee.org

Funding information
European Regional Development Fund, Grant/Award Number: Sêr Cymru II 80761-BU-103

Abstract

This paper proposes an extended state observer (ESO)-based second-order sliding mode control (SMC) for dynamic voltage restorers (DVRs). Unlike the conventional first-order SMC and some second-order SMC (SOSMC) methods that suffer from chattering, the proposed control method can alleviate chattering and achieve finite-time convergence. Chattering suppression (i.e. eliminating discontinuities) is achieved via continuous control input which is also used to generate the pulse width modulation signals. However, while removing the discontinuities in the control input, the performance of the control method is degraded when it is subjected to disturbances. Therefore, an active disturbance rejection (ADR) based on an ESO is proposed to enhance the performance. In addition, an advanced single-phase phase-locked loop (PLL) using linear observer and quasi-type-1 PLL is also proposed. The effectiveness of the proposed method is verified through simulation and experimental results which are compared with the results of the existing SMC methods applied to DVR.

1 | INTRODUCTION

The power quality degradations caused by power interruption, voltage sag, voltage swell, and harmonic distortion have attracted tremendous interest due to their detrimental effects on sensitive loads. To mitigate these disturbances, active filters based on power electronic custom devices are introduced in literature [1, 2]. The resilient control of such devices with the aim of injecting the desired compensating voltage (or current) into the grid is extremely important. A dynamic voltage restorer (DVR) is a series compensation device that compensates the voltage disturbances by injecting a compensating voltage to the point of common coupling (PCC) [3]. With the aim of protecting sensitive loads from such disturbances, numerous studies are carried out on the topology and control (linear or non-linear) of DVRs [4–14]. The proposed controllers in the literature are based on optimized proportional-integral (PI) controllers [4], feedback theory [5, 6], repetitive control [7], and sliding mode control (SMC) methods [8–14].

However, the non-linear control methods are more effective than the linear ones in achieving the desired dynamic response and robustness (insensitivity to parameter variations and disturbances) due to the non-linearity of the model of the custom power devices. One of the most popular non-linear control methods is the SMC method. This method offers significant advantages such as the minimum steady-state error, fast dynamic response, and disturbance (internal or external) rejection. In addition, its implementation in practice is easy since it does not need the mathematical model of the system. However, it suffers from the high-frequency fluctuations in the control input referred to as the chattering which is not preferred in practice.

Although the conventional first-order SMC method applied to DVR has strong robustness, it is not able to achieve chattering suppression entirely [8, 9]. In [10], a pseudo-SMC based on the boundary layer method is introduced to eliminate the effect of chattering. Nevertheless, the boundary layer method is a tradeoff between the steady-state error and the chattering. Moreover, due to the requirement for the relative degree of the sliding variable to be equal to one, it needs the derivative of the state variable. In addition, in a linear sliding manifold, the state variables converge to the origin asymptotically. One of the

effective chattering mitigation methods proposed recently is the high-order SMC method [11, 15–17]. Unlike the conventional first-order SMC that should be designed for a system with relative degree one, the high-order SMC can be designed with higher relative degree sliding manifolds [15]. Since most of the practical systems are of second or higher order, it is reasonable to use a higher-order SMC method instead of the conventional first-order one. The second-order SMCs (SOSMCs) available in the literature have also discontinuities in the control input and need a derivative of the state variable [16]. Even though the super twisting SMC (STSMC) is one of the SOSMCs introduced to diminish the chattering effect, it has a constraint of relative degree which should be equal to one for the sliding variable design. In [11], the idea of STSMC is successfully applied to DVR. However, this method has three drawbacks:

(i) Unlike other SOSMCs, this method can only be applied to a system with relative degree one (i.e. same as the conventional SMC). This means that the control input should appear in the first derivative of the sliding variable [17].
(ii) It does not have a satisfactory dynamic response under disturbances due to steady-state error. Moreover, if one chooses a linear surface, then the states converge to the origin asymptotically [18].
(iii) The control parameter tuning is very complicated due to the dependence on the derivative of disturbance boundaries. Hence, the control parameters are determined by the trial-and-error method [19].

On the other hand, in the case of a linear sliding manifold, the state variables have asymptotic convergence while the system requires an input relative degree equal to one. However, the non-linear sliding surface attains finite-time convergence without having any restriction on the relative degree [20]. For achieving both the finite-time convergence and chattering elimination for a double integrator system, Levant suggested a third-order SMC [15]. However, this method needs exact information on uncertainties due to the third state which complicates the design.

Nevertheless, the conventional SMC is a high-performance controller under various uncertainties, but it is vulnerable to distortion and uncertainties when chattering alleviation methods are applied to the system. To diminish the effect of such uncertainties, active disturbance rejection (ADR) controllers have been embedded in the SMC method in recent studies [21–25]. A crucial benefit of this new scheme is that it can handle the uncertainties through an extended state observer (ESO) by estimating the disturbances and compensating them in a feedforward way. The combination of the ESO and SMC to observe the disturbances in the system and feedback on the SMC scheme is mostly applied to the permanent magnet synchronous motors (PMSM) for speed control [21–23, 25]. However, these strategies use the conventional SMC with a sign function in the control input which is a robust system itself that can handle the uncertainties effectively and the ESO seems unnecessary. On the other hand, the system suffers from chattering and high-frequency noises due to the non-smoothed control input. Furthermore, a finite-time adaptive ESO-based dynamic SMC for hybrid robots has been proposed in [24] which is suffering from chattering due to the discontinuous control input. Hence, a finite-time convergence SMC method with continuous control input as well as strong robustness under high uncertainties is not explored yet.

Therefore, this study intends to combine a chattering-free non-linear SMC combined with an ESO to address both uncertainties and discontinuity of the conventional SMC.

Furthermore, an important part of the overall DVR control system is the generation of the reference voltage. In the ideal setting, the measured grid voltage can be directly used to generate the unit voltage template. However, in practice, the grid voltage is often corrupted with harmonics and noise. Moreover, grid frequency is also variable. To address these issues, phase-locked loop (PLL) is often considered a suitable choice for generating the unit template from the measured grid voltage. Conventionally, synchronous reference frame PLL (SRF-PLL) is the most popular choice [26]. However, this PLL is only applicable for three-phase systems. In the case of single-phase system, that is, our case, an additional quadrature signal generator is required. There are numerous solutions available in the literature. Out of them, linear observer [27] can be considered a suitable choice. This method is easy to implement and tune. Once the quadrature signal is generated, the implementation of SRF-PLL is straightforward. However, SRF-PLL cannot be made fast enough without sacrificing the harmonic robustness. Unlike SRF-PLL, quasi type-1 PLL (QT1-PLL) [26, 28] can address this issue as it has a simpler lower-order loop filter structure. As such, this approach has been selected in our work.

Considering the dynamic response advantage of QT1-PLL, several PLL methods involving this architecture have been proposed in the literature [29–35]. However, most of them [29–32, 35] are dedicated to the three-phase systems. To the best of our knowledge, very few results are available for the single-phase case. In [33], a QT1-type open-loop estimator has been proposed for the single-phase system. This system is suitable for grid monitoring purposes. However, when it comes to utilizing this method in a closed-loop converter control, the implementation can be tricky due to the lack of a small-signal model. In addition, several filters and correction factors need to be calculated in real time, which further increases the real-time implementation complexity. In [34], a frequency-fixed all-pass filter (APF)-based QT1-PLL has been proposed. This method can eliminate DC offset and provides good harmonic robustness. However, it has higher computational complexity. It uses a half-cycle delayed signal cancellation block for DC offset elimination and two half-cycle moving average filters for odd-order harmonics rejection. This significantly increases the memory requirement. In addition, due to the use of frequency fixed APF, additional amplitude and phase corrections are also needed to be implemented in real time. To address the limitations of existing single-phase QT1-PLLs, a simple structure is considered here. First, a frequency adaptive Luenberger observer is used as the quadrature signal generator. Unlike similar methods such as second-order generalized integrator (SOGI) [36], the Luenberger observer does not use estimated frequency in the output error injection term. This makes the observer less sensitive to frequency variation, compared to SOGI. Secondly, to provide

harmonic robustness, a low-pass filter is used as opposed to the conventionally used moving average filters. This lowers the computational burden of the proposed method over similar techniques from the literature [33, 34].

Therefore, the contributions of our paper can be listed as

1. An SOSMC with a chattering alleviation feature and non-linear sliding variable is introduced in this paper. Different from the recent method [12] which suffers of stability under transient disturbances, the proposed method strengthens the robustness of the scheme under disturbances with an ADR capability based on ESO to estimate the disturbances and improve the performance of the strategy.
2. The proposed SOSMC is designed based on the non-linear sliding manifold which is a kind of terminal SMC that achieves finite time convergence of the states. Contrary to the recent studies [37] which are utilizing a linear sliding manifold, the proposed method converges to the new setpoint under dynamic situations in less time.
3. On the contrary to the recent studies [23] which are using ESO with the conventional SMC to strengthen the robustness of the scheme, but are suffering of the chattering, the proposed control method in this study is based on an integral of the sign function to smooth the control input and alleviate the chattering effect while also the robustness is guaranteed by a disturbance rejection method.
4. A single-phase quasi type-1 PLL (QT1-PLL) using a Luenberger observer is proposed as the quadrature signal generator. Conventionally, QT1-PLL is only applicable to three-phase systems. So, the novelty of the proposed PLL is the extension of the three-phase system to a single-phase system. Moreover, the small-signal model and constructive gain tuning procedure are also discussed. On the other hand, the proposed single-phase QT1-PLL can provide good robustness against harmonics.

The paper is organized as follows. Section 2 presents the mathematical model of DVR. Section 3 introduces the basic concepts of the ADR with ESO. Section 4 outlines the main second-order SMC design methods. Section 5 describes the PLL-based reference voltage generation. Section 6 describes the simulation and experimental results and finally Section 8 concludes the paper.

2 | MATHEMATICAL MODEL OF DVR

Figure 1 shows a single-phase DVR injecting a voltage between the grid and load for compensating the voltage fluctuations in the grid. The voltage injection is done through a transformer (T) which isolates the DVR from the grid. The mathematical model of the system can be written as

$$\begin{aligned} L_f \frac{di_f}{dt} + r_f i_f &= v_i - v_c \\ C_f \frac{dv_c}{dt} &= i_f - i_g \end{aligned} \tag{1}$$

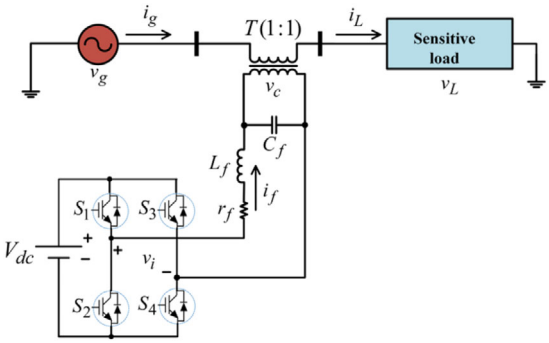

FIGURE 1 Single-phase DVR. DVR, dynamic voltage restorer.

where i_g is the grid current, i_f is the inductor current, v_c is the compensating voltage, L_f and C_f are the filter inductor and capacitor and r_f is the resistor related to L_f, respectively. Considering $v_i = uV_{dc}$, $x_1 = v_c - v_c^*$ and $x_2 = \dot{x}_1$, one can obtain the following state space equations:

$$\begin{aligned} \dot{x}_1 &= x_2 \\ \dot{x}_2 &= F + b_o u \end{aligned} \tag{2}$$

where u is the control input, v_c^* is the compensating voltage reference and $F = \rho_1 + \rho_2$ is the lumped disturbance of the system defined as the summation of the internal and external disturbances given by

$$\rho_1 = -\omega_o^2 x_1 - \frac{r_f}{L_f} x_2 \tag{3}$$

$$\rho_2 = -\omega_o^2 v_c^* - \frac{di_g}{C_f dt} - \frac{r_f}{L_f}\frac{dv_c^*}{dt} - \frac{d^2 v_c^*}{dt^2} - r_f \omega_o^2 i_g \tag{4}$$

where ${\omega_o}^2 = 1/L_f C_f$ and $b_o = {\omega_o}^2 V_{dc}$. It is assumed that the lumped perturbation is bounded by a known function as follows:

$$|F = \rho_1 + \rho_2| \le \mu \tag{5}$$

The disturbance of the system is in the class of the matched disturbances which can be circumvented through the conventional SMC entirely. However, the chattering still exists, and state convergence is asymptotical [16].

3 | ACTIVE DISTURBANCE REJECTION WITH EXTENDED STATE OBSERVER

The active disturbance rejection control (ADRC) method is a robust control scheme based on the extension of the system model while creating a fictitious state variable. This virtual state variable is a delegate of the whole uncertainty and disturbances that have not been included in the model of the system. Then the method is leveraging a state observer to estimate the virtual state and then uses it in the control loop in order to

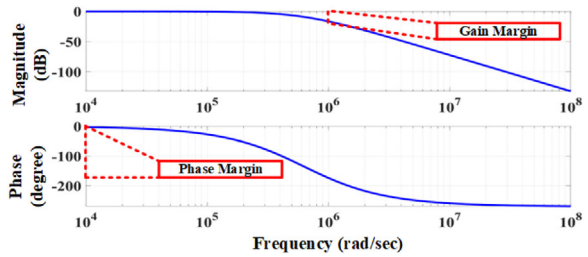

FIGURE 2 Bode plot of the transfer function (8).

decouple the system from the actual perturbation existing in the system. The ESO used in this study is a kind of ADRC method which is not only to observe and estimate disturbances and eliminate them in the control law but also to estimate the second state variable without the requirement for calculating it in the control loop using the derivative operator or an extra sensor.

By applying the ESO, F can be estimated based on the following state space model:

$$\begin{bmatrix}\dot{\hat{x}}_1\\ \dot{\hat{x}}_2\\ \dot{\hat{F}}\end{bmatrix}=\begin{bmatrix}0&1&0\\0&0&1\\0&0&0\end{bmatrix}\begin{bmatrix}\hat{x}_1\\ \hat{x}_2\\ \hat{F}\end{bmatrix}+\begin{bmatrix}0\\ b_o\\ 0\end{bmatrix}u+\begin{bmatrix}\alpha_1\\ \alpha_2\\ \alpha_3\end{bmatrix}e \tag{6}$$

where $e=\hat{x}_1-x_1$ and $L=[\alpha_1,\alpha_2,\alpha_3]$ is the observer gain vector. Obviously, the observer assigns the disturbances a third state variable and estimates all disturbances. The observer gain vector can be derived by using pole placement assignment methods. The observer parameter tuning is considered in such a way to have a tradeoff between the least sensitivity to noise and fast response. In [38] and [39], the gains are selected as follows:

$$\alpha_1=3\omega_s,\alpha_2=3{\omega_s}^2,\alpha_3={\omega_s}^3 \tag{7}$$

where ω_s is the observer bandwidth that can be determined on the basis of inverter system bandwidth. In this paper, $\omega_s=2\pi f_s$ where f_s is the sampling frequency. If the observer gains are computed according to (7) and substituted into (6), then the transfer function from $\ddot{x}_1$ to $\hat{F}$ can be derived as follows:

$$T_{ESO}=\frac{\omega_s^3}{(s+\omega_s)^3} \tag{8}$$

Equation (8) is a low pass filter with three poles located at the left-half of s-plane proving the stability of ESO. To further assure the stability of the designed ESO for the DVR the bode plot of the transfer function given in (8) is depicted in Figure 2. Obviously one can see that both gain margin and phase margin of the proposed transfer function determine the stability of the proposed disturbance rejection observer.

4 | SECOND-ORDER SLIDING MODE CONTROL

The design of the SMC is based on formulating the sliding manifold and selecting a control input such that the existence of the sliding mode is assured. In the case of DVR control, the reference compensating voltage can be obtained by subtracting the measured grid voltage from the reference load voltage as follows:

$$v_c^*=v_L^*-v_g \tag{9}$$

where v_L^* is the reference load voltage. It is apparent that $v_c^*=0$when there is no fluctuation in the grid voltage (i.e. $v_g=v_L^*$).

Now, let the non-linear sliding function be defined as follows:

$$S=\alpha|x_1|^{\lambda}sign(x_1)+\dot{x}_1 \tag{10}$$

where $x_1\in\mathbb{R}$ is the state variable, $\alpha>0$, and $0<\lambda<1$. Obviously, one needs either a differentiator to obtain a high accuracy estimation of $\dot{x}_1$ or by measuring the capacitor current and multiplying it by $\frac{1}{C_f}$. Clearly, following the second method needs the circuit parameters and disrates the robustness of the system while it needs another current sensor to measure the capacitor current. Thus, considering (2) and (6), the estimation of $\dot{x}_1$can be easily substituted into (10) as previously has been derived by the ESO method. Moreover, in a non-linear sliding variable, there is no need to consider the relative degree for designing the control input. The addition of the term $|x_1|^{\lambda}sign(x_1)$augments the convergence on the road to the equilibrium point. The closer to the equilibrium, the faster the convergence, leading to finite-time convergence. The reaching time is adjustable by tunning parameters λ and α.

Taking the first derivative of (10) and making use of the estimated state variables, one can obtain

$$\begin{aligned}\dot{\hat{S}}&=\alpha\lambda\dot{x}_1sign(x_1)|x_1|^{\lambda-1}+\dot{\hat{x}}_2\\&=\alpha\lambda(\hat{x}_2)sign(x_1)|x_1|^{\lambda-1}+\hat{F}+b_ou+\alpha_2e\end{aligned} \tag{11}$$

Thus, the control input can be designed as follows:

$$u=u_{eq}+u_{sw} \tag{12}$$

where u_{eq} and u_{sw} denote the equivalent control and switching control, respectively. The equivalent control is derived from $\dot{\hat{S}}=0$ as follows:

$$u_{eq}=b_o^{-1}(-\alpha\lambda(\hat{x}_2)sign(x_1)|x_1|^{\lambda-1}-\alpha_2e-\hat{F}) \tag{13}$$

Thanks to the ESO mentioned before, the disturbance term ($\hat{F}$) estimated from (6) can be substituted into (13) to compensate the disturbances in the system. Thus, the closed form of

(13) is as follows assuming that $\hat{F}(0) = 0$.

$$u_{eq} = b_o^{-1}(-\alpha\lambda(\hat{x}_2)sign(x_1)|x_1|^{\lambda-1} - \alpha_2 e - \int_0^{\tau} \alpha_3 e d\tau) \quad (14)$$

The switching control input is considered as follows:

$$u_{sw} = -k\int_0^{\tau} sign(\hat{S})d\tau \quad (15)$$

where k is the switching control input constant which can be selected through the existence condition rules. According to [15] the chattering can be significantly diminished by inserting an integrator in the controller provided that the sliding manifold and its derivatives are kept close to zero. Hence, the main aim of the switching control is to suppress the chattering. To prove the finite time convergence, one can equalize the sliding variable ($\hat{S}$) to zero which results:

$$\hat{x}_2 = -\alpha|x_1|^{\lambda} sign(x_1) \quad (16)$$

Since in the steady state all the estimation errors converge to zero, therefore the estimation error (e) will converge to zero in the steady state and $\hat{x}_2 = x_2 = \dot{x}_1$. Substituting $sign(x_1) = \frac{{x_1}^{\lambda}}{|x_1|^{\lambda}}$ into (16) yields

$$\dot{x}_1 = -\alpha {x_1}^{\lambda} \quad (17)$$

Therefore, the time (t_r) taken for x_1 to travel from the initial point ($x_1(t_0)$) to equilibrium is given by

$$t_r = \frac{1}{\alpha(1-\lambda)}\left|x_1(t_0)\right|^{(1-\lambda)} \quad (18)$$

Equation (18) means that $x_1$can converge to zero in finite time. Also, due to the relation of x_1 and $x_2$in (2), $x_2$travels to equilibrium point in finite time similarly.

Selecting the parameter λ in the sliding variable in (10) is thoroughly aimed in such a way to minimize the reaching time. As (18) shows, the reaching time is dependent on the initial value of the state variable ($x_1(t_0)$) and αwhich is called the sliding coefficient. To pick the optimum value for λ, the minimum reaching time occurs when the derivative of the reaching time in terms of λ is zero.

$$\frac{dt_r}{d\lambda} = \frac{\left|x_1(t_0)\right|^{(1-\lambda)}}{\alpha}\left(\frac{1}{(1-\lambda)^2} - Ln\left(\left|x_1(t_0)\right|\right)\right) = 0 \quad (19)$$

Evaluating (19) displays that the suitable value for λ is dependent on the initial value of the state variable. In the proposed method the appropriate value for λ is selected equal to 0.5 based on the initial value of the state variable.

To prove the stability of the proposed controller, a Lyapunov function candidate is defined as

$$V = \frac{\hat{S}^2}{2} \quad (19)$$

For stability, the derivative of the Lyapunov function should satisfy

$$\dot{V} = \hat{S}\dot{\hat{S}} < 0 \quad (20)$$

Substituting (13) and (15) as the control input into (20) the closed form of the inequality yields

$$\begin{aligned}\hat{S}\dot{\hat{S}} &= \hat{S}\left(\frac{\alpha}{2}(\hat{x}_2)sign(x_1)|x_1|^{-\frac{1}{2}} + \hat{F} + b_o u + \alpha_2 e\right) < 0\\ &= \hat{S}\left(b_o u_{sw} + \hat{F} - \int_0^{\tau}\alpha_3 e d\tau\right)\\ &< -\left|\hat{S}\right|\left(b_o k\int_0^{\tau} sign(\hat{S})d\tau < -b_o k\left|\hat{S}\right|^2 < 0\right.\end{aligned} \quad (21)$$

where $\int_0^{\tau} sign(\hat{S})d\tau < |\hat{S}|$ and $\hat{F} = \int_0^{\tau}\alpha_3 e d\tau$. Therefore, the closed-loop designed control system has finite time stability. On the other hand, considering any positive parameter for k can guarantee the stability of the system whereas this coefficient plays a role in improving the stability of the system and reaching time; it is also responsible for alleviating the chattering in the control input.

5 | PLL-BASED REFERENCE VOLTAGE GENERATION

The load voltage reference should be generated as follows:

$$v_L^* = V_L^* \sin(\theta) \quad (22)$$

where V_L^* is the targeted reference amplitude of the load and θ is the phase angle which should be synchronized with v_g. Thus, in order to synchronize v_L^* with v_g, the following PLL strategy is proposed in this section.

A single-phase grid voltage can be written as

$$v_g(t) = y = V_g\cos(\omega_g t + \phi_g) \quad (23)$$

where the amplitude, frequency and phase are denoted by V_g,ω_g and, $\phi_g$respectively. Instantaneous phase in (23) can be defined as $\theta_{\partial g} = \omega_g t + \phi_g$. To ensure efficient operation of the DVR, estimation of $\sin(\theta_g)$ (i.e. unit sine template) is essential. For this purpose, a QT1-PLL with low-pass filter is considered in this work [26, 28]. Actually, the QT1-PLL is designed for the three-phase system. In the single-phase case, only one signal is available for measurement. As such, the generation of the quadrature signal is required. This is considered below.

5.1 | Quadrature signal generator (QSG)

To generate the quadrature signal, let us consider that $y = v_\alpha$ and $y_\beta = v_\alpha^\perp = V_g \sin(\theta_g)$. Then, the state-space model of the grid voltage can be found as

$$\dot{\xi} = A\xi \tag{24}$$

$$y = C\xi \tag{25}$$

where $\xi = [v_\alpha\, v_\beta]^T$, $A = \begin{bmatrix} 0 & -\omega_g \\ \omega_g & 0 \end{bmatrix}$ and $C = \begin{bmatrix} 1 \\ 0 \end{bmatrix}^T$. For system (24) and (25), estimating the quadrature signal y_β from y is an essential problem of designing an appropriate observer/filter. In this work, the Luenberger observer is considered for system (24) and (25) as follows [40]:

$$\dot{\hat{\xi}} = A\hat{\xi} + L(y - C)\hat{\xi} \tag{26}$$

$$\hat{y} = C\hat{\xi} \tag{27}$$

where $\hat{}$ denotes estimated values and $L = [l\ 0]^T$, $l > 0$. The transfer functions of the estimated variables are given by

$$\frac{\hat{v}_\alpha}{y}(s) = \frac{ls}{s^2 + \omega_g s + \omega_g^2} \tag{28}$$

$$\frac{\hat{v}_\beta}{y}(s) = \frac{l\omega_g}{s^2 + \omega_g s + \omega_g^2} \tag{29}$$

The second-order transfer functions (28) and (29) show that the linear observer has band-pass filtering characteristics and there is a 90° phase difference between the estimated variables. This is very useful for grid-synchronization application where harmonics are often present. Band-pass filtering helps to extract the fundamental component from the harmonically distorted grid voltage signal. By assuming $\phi_g = 0$, the time-domain response of the transfer functions (28) and (29) is given by

$$\hat{v}_\alpha(t) = V_g \cos(\theta_g) - V_g e^{\frac{-lt}{2}} (\cosh(tl^*) - l \sinh(tl^*)/2l^*) \tag{30}$$

$$\hat{v}_\beta(t) = V_g \sin(\theta_g) - V_g e^{\frac{-lt}{2}} (\omega_g \sinh(tl^*)/l^*) \tag{31}$$

where $l^* = \sqrt{(l/2)^2 - \omega_g^2}$. Time domain responses in (30) and (31) show that both equations have an exponential decay rate of $l/2$. As such, as $t \to \infty$, the estimates will become equal to the actual values. So, by tuning the gain l, the convergence time of the observer can be manipulated. Due to the presence of the exponential decay term, the dynamics of the Luenberger observer can be approximated by a first-order low-pass filter (LPF) as

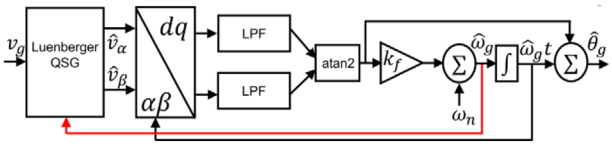

FIGURE 3 Block diagram of the proposed single-phase QT1-PLL. QT1-PLL, quasi-type-1 phase-locked loop.

$$G_{QSG}(s) = \frac{1}{(\tau_l s + 1)} \tag{32}$$

where the time constant is given by $\tau_l = 2/l$. It is well known that the settling time t_s of a first-order transfer function (29) is given by $4\tau_l$. Then, the gain l can be tuned by using the following formula:

$$l = \frac{8}{t_s} \tag{33}$$

It is to be noted here that in developing the Luenberger observer, it is assumed that the grid frequency ω_g is known. In practice, this value is unknown and a PLL can be used to estimate the grid frequency in real time.

5.2 | Implementation in QT1-PLL

The block diagram of the QT1-PLL with the QSG developed in Section 5.1 is given in Figure 3. Filtered signals $\hat{v}_\alpha$ and $\hat{v}_\beta$ can be directly used in the QT1-PLL. In the case of conventional SRF-PLL [40], the estimated phase $\hat{\theta}_g$ is used as the input to the Park transformation to obtain the dq−axis voltages. In the case of QT1-PLL, the time integral of the estimated frequency is used. As such, the phase detector of QT1-PLL works by estimating the phase angle ϕ_g. The outputs of the QT1-PLL phase detector are given by [28]

$$v_d = V_g \cos(\phi_g) \tag{34}$$

$$v_q = V_g \sin(\phi_g) \tag{35}$$

Then, the phase can be estimated as

$$\hat{\phi}_g = a\tan 2(v_q, v_d) \tag{36}$$

where $a\tan 2$ is the double-quadrant arc-tangent operation. To enhance the filtering performance of QT1-PLL, low-pass filter with cut-off frequency ω_c is considered at the output of v_d and v_q. Following Figure 3 and the QSG dynamics (32), small signal model of the proposed PLL can easily be obtained and given in Figure 4. The open- and closed-loop transfer functions of the

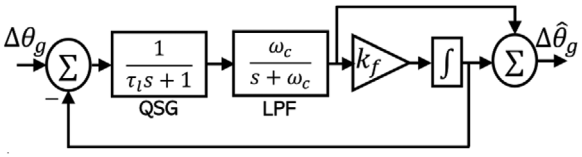

FIGURE 4 Small-signal model of the proposed PLL. PLL, phase-locked loop.

proposed PLL can be obtained as

$$G_{OL}(s) = \frac{\frac{1}{\tau_l s+1}\frac{\omega_c}{s+\omega_c}\frac{k_f+s}{s}}{1-\frac{1}{\tau_l s+1}\frac{\omega_c}{s+\omega_c}} = \frac{\omega_c s+k_f\omega_c}{\tau_l s^3+(\tau_l\omega_c+1)s^2} \tag{37}$$

$$G_{CL}(s) = \frac{\omega_c s+k_f\omega_c}{\tau_l s^3+(\tau_l\omega_c+1)s^2+\omega_c s+k_f\omega_c}, \tag{38}$$

Transfer functions (37) and (38) are useful for gain tuning and stability analysis purposes.

5.3 | Parameter tuning

The proposed PLL has three parameters to tune. They are QSG gain l, low-pass filter cut-off frequency ω_c and the frequency estimation dynamics gain k_f. Tuning of l can be done using formula (33). For this purpose, one-cycle settling time can be chosen as a good value for t_s, that is, $t_s = 0.02$. This results in $l = 400$ according to (33). To tune the LPF cut-off frequency, analogy with the moving average filter can be considered. In the case of MAF, half cycle window length can eliminate all the odd-order harmonic components. The first-order Pade approximation of MAF has the same transfer function as that of LPF and is given by

$$G_{MAF}(s) \approx \frac{2/T_\omega}{s+2/T_\omega} \tag{39}$$

where T_ω is the window length. By comparing (39) with that of low-pass filter, the cut-off frequency can be found as

$$\omega_c = 2/T_\omega \tag{40}$$

For $T_\omega = 0.01$ (half-cycle with 50-Hz fundamental frequency), one can find that $\omega_c = 200$rad/s. To tune the frequency estimation gain k_f, open-loop phase margin can be considered.

In the control system literature, open-loop phase margin in the range of $30° - 60°$is recommended. In this work, we are considering the middle point which is 45°. Open-loop phase margin calculated using (37) as a function of k_f can be found in Figure 5. Accordingly, it can be seen that k_f= 62 corresponds to phase margin of 45°. As such, this value has been selected. This completes the gain tuning process of the proposed PLL.

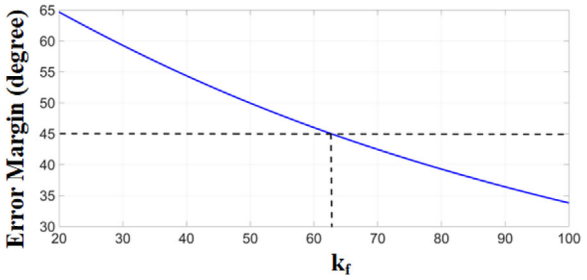

FIGURE 5 Phase margin of (38) as a function of k_f with $l = 400$and $\omega_c = 200$ rad/s.

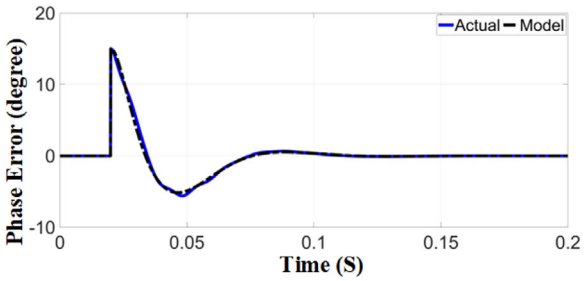

FIGURE 6 Closed-loop small-signal model (38) validation with, $l = 400$ $\omega_c = 200$ and $k_f = 62$.

5.4 | Small-signal model validation

To validate the small-signal model of the proposed PLL, a phase step change of +15°is considered. Figure 6 shows that the developed small-signal model (38) very closely follows the actual response with the selected tuning parameter values. This shows that the proposed model is very accurate. As such, local stability of the PLL with selected parameters can be ensured.

6 | SIMULATION AND EXPERIMENTAL RESULTS

The performance of the proposed method with the block diagram shown in Figure 7 is investigated through MATLAB/SIMULINK platform and experimental studies. The system and control parameters used in these studies are listed in Table 1. The DVR is built by using Mitsubishi CM 200DY-12H IGBT modules and associated driver circuits. The dc input of DVR has been obtained from a power supply. The voltages v_g and v_c are measured by using LEM LV25-P. The proposed SOSMC method is implemented via TMS320F28379D in which the measured signals are digitized by using built-in analog-to-digital converter and processed in compliance with Figure 8.

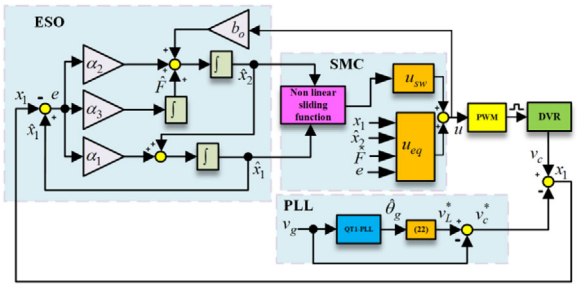

FIGURE 7 Block diagram of the proposed control method.

TABLE 1 System and control parameters.

Description and symbol	Value
Grid voltage and frequency (v_g,f_g)	120 V(rms), 50 Hz
DC link voltage (V_{dc})	120 V
Inductance and capacitance (L_f,C_f)	0.8 μH, 50 μF
α_1 , α_2 , α_3	3×10^4, 3×10^8, 10^{12}
Switching frequency (f_{sw})	10 kHz
Observer bandwidth (ω_o)	$2\pi\times10^5$
Sliding and integral gains (α, k)	10,000, 5000

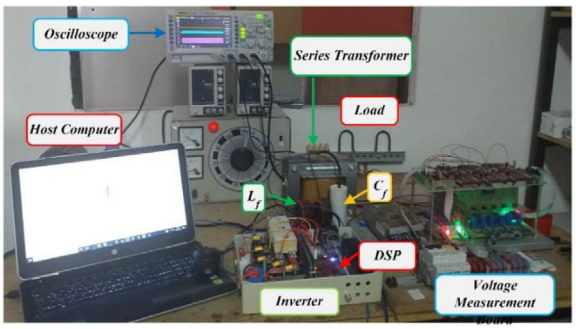

FIGURE 8 Experimental setup of the single-phase DVR. DVR, dynamic voltage restorer.

The efficiency of the proposed control method under three different anomalies which are sag, swell and distorted grid voltage is analyzed in the simulation platform of MATLAB. The results are described in Figures 9–11. The mentioned anomalies are analyzed when the system is connected to a resistive load and also connected to an inductive load to show that it can perform successfully under various loads.

The waveforms of grid voltage (v_g), compensation voltage (v_c), load voltage (v_L) and load current (i_L) are shown in Figure 9 when voltage sag occurs in the grid varying the grid voltage from 120 to 60 V (rms).

Figure 9a shows the waveforms while the system is connected to a resistive load ($R = 100\ \Omega$). It is apparent that DVR does not inject any compensating voltage when there are no disorders in the grid voltage but as far as the voltage sag arises in the grid, the DVR replies instantly by generating a compensation voltage so that the load voltage is not affected from the voltage sag. The

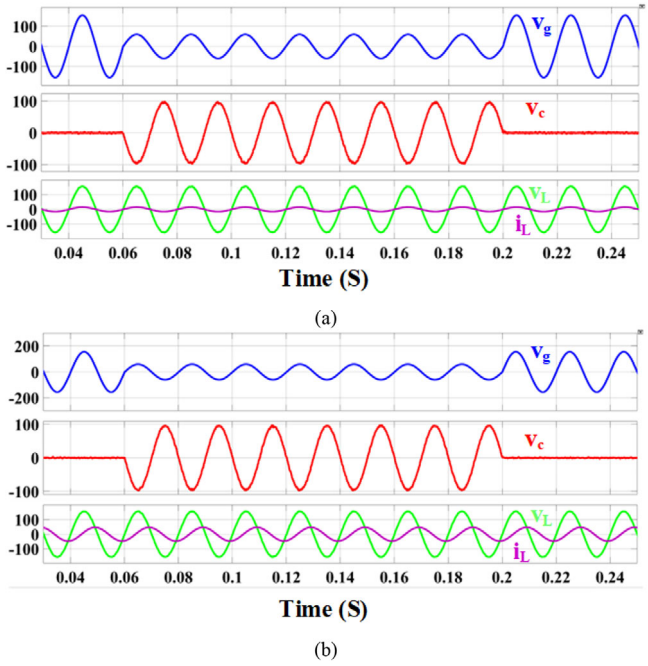

FIGURE 9 Waveforms obtained for voltage sag under: (a) resistive load, (b) RL load.

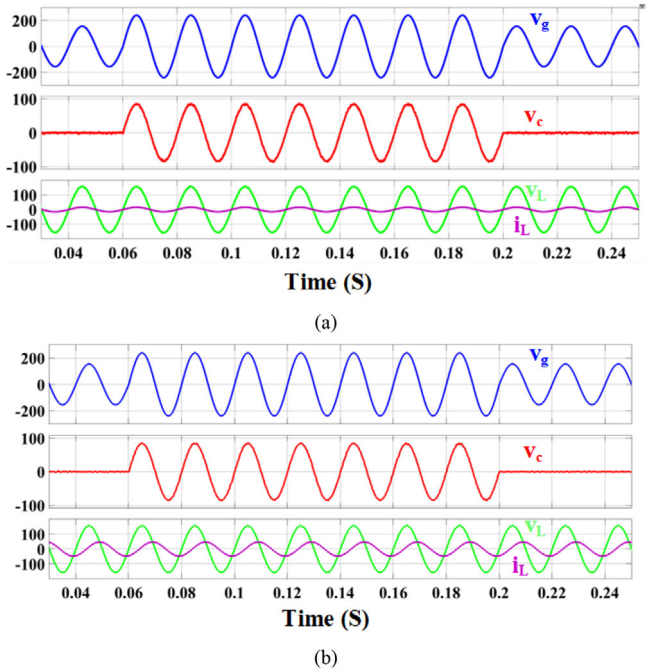

FIGURE 10 Waveforms obtained for voltage swell under: (a) resistive load, (b) RL load.

compensation voltage becomes zero again when the sag period is over.

It is worth mentioning that because the load is resistive under all transient time slots both load current and load voltage are in phase.

Same waveforms for voltage sag under inductive load ($100\Omega + 1H$) are given in Figure 9b. Clearly, the load voltage

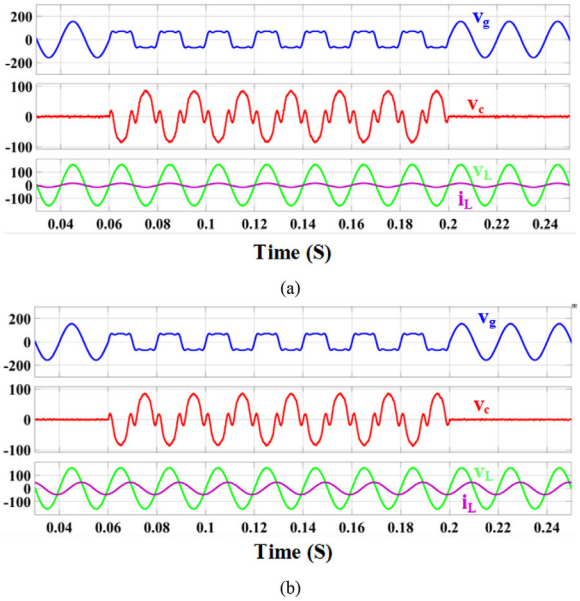

FIGURE 11 Waveforms obtained for distorted grid voltage: (a) resistive load, (b) RL load.

is not affected from the voltage sag that occurred in the grid voltage. The load current lags the load voltage due to the RL load.

The waveforms of grid voltage (v_g), compensation voltage (v_c), load voltage (v_L) and load current (i_L) are shown in Figure 10 when voltage swell occurs in the grid varying the grid voltage from 120 to 240 V (rms).

The system under the voltage swell is tested for both resistive and inductive loads and the results are given in Figures 10a and 10b, respectively. The behaviour of DVR under voltage swells when only resistive load ($R = 100\ \Omega$) is connected to the load side is shown in Figure 10a. Obviously, the DVR injects compensating voltage when the disturbance occurs and stops generating when the disorder in the grid disappears. On the other hand, the load current and voltage are also in phase due to the resistive load. The results of the voltage swell under inductive load ($100\Omega + 1H$) are shown in Figure 10b. The voltage swell lasts for seven cycles and DVR acts in such a way that the load voltage is not affected from the voltage swell of the grid.

On the other hand, having a load current waveform which lags the voltage waveform under inductive load proves that the DVR is working successfully under various types of loads.

To evaluate the behaviour of the DVR and the performance of the proposed control method under a distorted grid voltage, the grid voltage is distorted by harmonics (harmonics with third, fifth and seventh orders) and the results are given in Figure 11. Figure 11a shows the reaction of the DVR under resistive load when the grid voltage is distorted. As one can see the load voltage is not affected from the grid side due to the swift reaction of the DVR in injecting the compensation voltage.

Furthermore, the performance of the DVR under inductive load ($100\Omega + 1H$) while instantly the grid is distorted by harmonics is shown in Figure 11b. Similarly, the system performs promptly to the disorders and keeps the load voltage sinusoidal under such a disturbance.

The experimental results of the voltage waveforms of v_c, v_g and v_L are depicted in Figure 12. Figure 12a shows the voltage waveforms under a 50% voltage sag from 120 to 60 V. The voltage swells which depict a variation from 120 to 144 V are shown in Figure 12b.

The effectiveness of the proposed control method under distorted grid voltage (harmonics with third, fifth and seventh orders) is also investigated as shown in Figure 12c. The amplitude of the harmonic components over the grid voltage is 15% of the fundamental value for the third harmonic, 10% of the fundamental value for the fifth harmonic and 5% of the fundamental for the seventh harmonic. Therefore, the total harmonic distortion (THD) of the grid voltage is 18.47%. Obviously, the proposed method is quite effective in generating a sinusoidal load voltage with THD = 1.18% and protecting the sensitive load from the hazards of the harmonics in the grid. The results in Figure 12 demonstrate that the proposed control method reacts to the disturbances in the grid and compensates the effects of these disturbances very fast and in finite time before they reach the load terminals.

Figure 13 shows the simulation results comparison of the proposed control method with STSMC under voltage sag with 50% decrement at $t = 0.065$ s. Conventionally, tunning the gains of the STSMC depends on the gradients of the disturbances appearing in the system, which is difficult to attain. Hence, to tune the gains of the STSMC method, the proposed approach in [17] is applied. The control inputs of STSMC and the proposed method are represented by U_S and U_P, respectively. Under approximately same chattering phenomena for both STSMC and the proposed method which is shown in Figure 13a, the convergence trajectory, and the steady state error of the STSMC, and proposed method are compared in this figure. Figure 13b compares the steady-state error for both methods. Clearly, the STSMC has a higher steady-state error than the proposed method under same chattering alleviation. Comparing the convergence trajectories in Figure 13c, one can see that the proposed method outperforms the STSMC in terms of response time under a disturbance thanks to the use of non-linear sliding manifold and ADR in the proposed method.

Table 2 displays a comparison between the typical SMC, STSMC and the proposed method. Considering the merits of the proposed method which are the finite-time response of the state variables, fixed switching frequency, robustness and not being restricted to the relative degree, this method outperforms the other conventional strategies.

To describe the effectiveness of the proposed PLL method, over the conventional second-order generalized integrator PLL (SOGI-PLL) [36] both methods are applied on the grid voltage under the proposed control strategy and the THD of the load voltage is calculated. The results of the THD of the load voltage under both methods are given in Figure 14. Obviously while the proposed method shows 1.18% THD in the load voltage, the THD of the SOGI method is higher which proves the privilege of the proposed PLL scheme in alleviating the harmonic distortions.

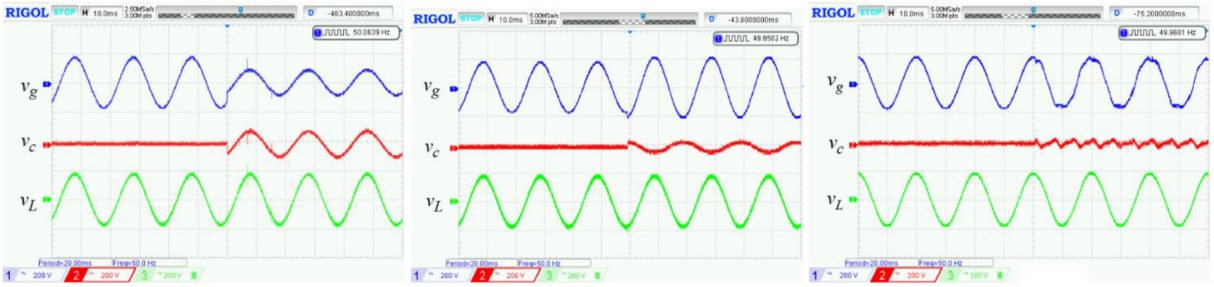

FIGURE 12 Dynamic responses of v_g, v_C and v_L under: (a) voltage sag, (b) voltage swell, (c) distorted grid voltage.

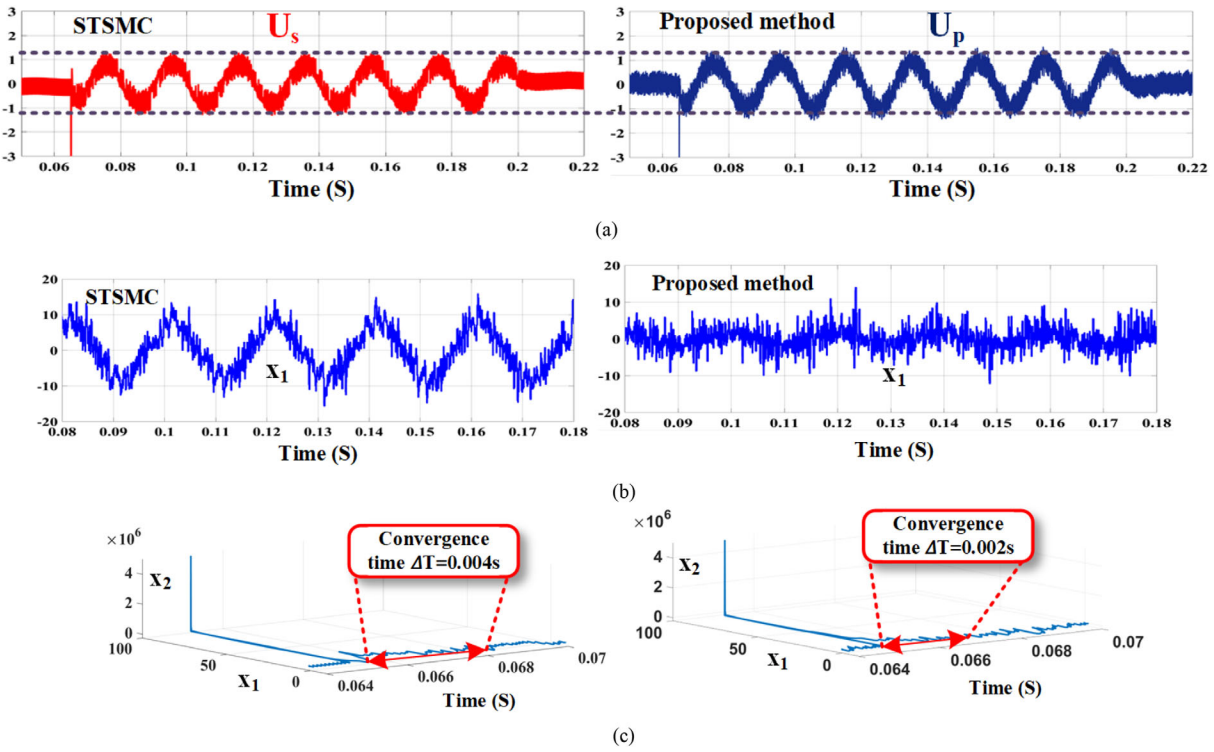

FIGURE 13 Comparison of the proposed method with the conventional STSMC under 50% voltage sag: (a) control input, (b) steady-state error, (c) convergence trajectory. STSMC, super twisting sliding mode control.

TABLE 2 Comparison of typical SMC, STSMC and proposed control methods.

Item	Typical SMC	STSMC	Proposed method
Control input signal	Discontinuous	Continuous	Continuous
Convergence	Asymptotic	Asymptotic	Finite time
Steady-state error	Zero	Exists	Almost zero
Disturbance rejection	No	No	Yes
Chattering suppression	No	Yes	Yes
Relative degree requirement	One	One	Not restricted to relative degree

SMC, sliding mode control; STSMC, super twisting sliding mode control.

Table 3 compares the existing SMC methods for DVR and the proposed SMC-based strategy. Obviously, one can see that the proposed method outperforms the others considering finite time convergence, zero steady-state error and continuous control input while it is leveraging a unique QT-1 PLL to synchronize the grid phase with the load reference voltage.

7 | CONCLUSION

In this paper, a second-order SMC combined with ADR is introduced for DVRs. It is shown that the proposed method suppresses the chattering and achieves finite-time convergence of the state variables. Furthermore, the steady-state error and robustness degradation arising due to the continuous nature of

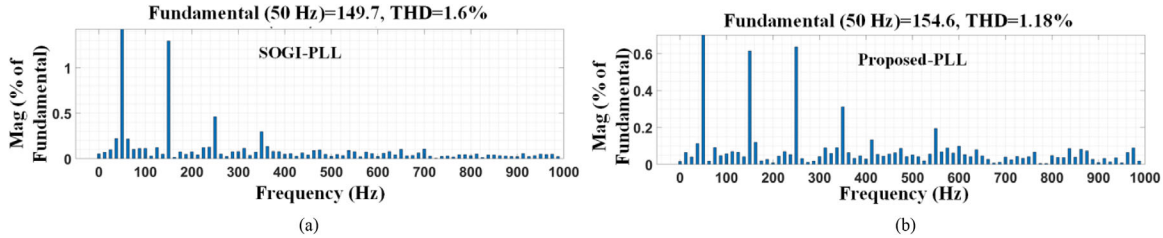

(a) (b)

FIGURE 14 Comparison of the THD of the load voltage under 50% voltage sag and harmonics in the grid voltage: (a) SOGI PLL, (b) proposed PLL. PLL, phase-locked loop; SOGI, second-order generalized integrator; THD, total harmonic distortion.

TABLE 3 Comparison of the existing SMC methods for DVR.

The applied method	[9]	[10]	[11]	[12]	[13]	[14]	[15]	Proposed method
Topology	1 phase-H bridge	3 phase–12-switch	3 phase– half bridge	1 phase-H bridge	3 Phase PWM chopper	1 phase 3-level T-type inverter	1 phase-H bridge	1 phase-H bridge
Number of sensors	3	3	2	3	3	4	4	2
Control input signal	Discontinuous	Discontinuous	Semi-continuous	Continuous	Discontinuous	Discontinuous	Not given	Continuous
Convergence	Asymptotic	Asymptotic	Asymptotic	Asymptotic	Asymptotic	Asymptotic	Asymptotic	Finite time
Steady-state error	Zero	Zero	Exists	Exists	Zero	Zero	Exists	Zero
Disturbance rejection	No	No	No	No	No	No	No	Yes
Chattering suppression	No	No	Yes	Yes	No	No	No	Yes
Robustness	Exists	Exists	Vulnerable	Exists	Exists	None	Yes	Yes
Grid synchronization method	PLL	Adaptive notch filter	Not applied	Brockett oscillator	SOGI-PLL	PLL	PLL	Quasi type-1 PLL

DVR, dynamic voltage restorers; PLL, phase-locked loop; SMC, sliding mode control; SOGI, second-order generalized integrator.

control input are eliminated by an ADR method based on an ESO. Moreover, the proposed single-phase QT-1 PLL method is offering good robustness against harmonics which is verified through the simulation results. Ultimately, the proposed method is compared with the STSMC method, and it is shown that the proposed scheme not only possesses easier parameter tuning, but also outperforms the STSMC method.

AUTHOR CONTRIBUTIONS

Farzaneh Bagheri: Conceptualization, Formal analysis, Investigation, Methodology, Software, Writing – original draft. Samet Biricik: Formal analysis, Investigation, Methodology, Software, Validation, Writing – review & editing. Hafiz Ahmed (GE): Conceptualization, Formal analysis, Funding acquisition, Methodology, Software, Writing – original draft. Hasan Komurcugil: Conceptualization, Methodology, Writing – review & editing

CONFLICT OF INTEREST STATEMENT

The authors declare no conflict of interest.

DATA AVAILABILITY STATEMENT

The data that support the findings of this study are available from the corresponding author upon reasonable request.

ORCID

Samet Biricik https://orcid.org/0000-0002-1559-2024
Hafiz Ahmed https://orcid.org/0000-0001-8952-4190
Hasan Komurcugil https://orcid.org/0000-0003-4728-6416

REFERENCES

1. Middlekauff, S.W., Collins, E.R.: System and customer impact: Considerations for series custom power devices. IEEE Trans. Power Delivery. 13(1), 278–282 (1998)
2. Brenna, M., Faranda, R., Tironi, E.: A new proposal for power quality and custom power improvement: OPEN UPQC. IEEE Trans. Power Delivery. 24(4), 2107–2116 (2009)
3. Abas, N., Dilshad, S., Khalid, A., Saleem, M.S., Khan, N.: Power quality improvement using dynamic voltage restorer. IEEE Access 8, 164325–164339 (2020)
4. Naidu, T.A., Arya, S.R., Maurya, R., Sanjeevikumar, P.: Variable fractional power-least mean square based control algorithm with optimized PI gains for the operation of dynamic voltage restorer. IET Power Electron. 14(4), 821–833 (2021)

5. Gao, S., Lin, X., Ye, S., Lei, H., Kang, Y.: Transformer inrush mitigation for dynamic voltage restorer using direct flux linkage control. IET Power Electron. 8(11), 2281–2289 (2015)
6. Li, P., Wang, Y., Wang, C., Lu, J., Pan, X., Blaabjerg, F.: Mitigation of voltage sag for DVR to comply with voltage security protocol via elliptical trajectory compensation. IET Power Electron. 14(5), 1044–1058 (2021)
7. Roncero-Sánchez, P., Acha, E.: Dynamic voltage restorer based on flying capacitor multilevel converters operated by repetitive control. IEEE Trans. Power Delivery. 24(2), 951–960 (2009)
8. Biricik, S., Komurcugil, H.: Optimized sliding mode control to maximize existence region for single-phase dynamic voltage restorers. IEEE Trans. Industr. Inform. 12(4), 1486–1497 (2016)
9. Biricik, S., Komurcugil, H., Tuyen, N.D., Basu, M.: Protection of sensitive loads using sliding mode controlled three-phase DVR with adaptive notch filter. IEEE Trans. Ind. Electron. 66(7), 5465–5475 (2019)
10. Komurcugil, H., Biricik, S.: Time-varying and constant switching frequency-based sliding-mode control methods for transformerless DVR employing half-bridge VSI. IEEE Trans. Ind. Electron. 64(4), 2570–2579 (2017)
11. Biricik, S., Komurcugil, H., Ahmed, H., Babaei, E.: Super twisting sliding-mode control of DVR with frequency-adaptive brockett oscillator. IEEE Trans. Ind. Electron. 68(11), 10730–10739 (2021)
12. Nasrollahi, R., Farahani, H.F., Asadi, M., Farhadi-Kangarlu, M.: Sliding mode control of a dynamic voltage restorer based on PWM AC chopper in three-phase three-wire systems. Int. J. Electr. Power Energy Syst. 134, 1–10 (2022)
13. Komurcugil, H., Bayhan, S., Guler, N., Abu-Rub, H., Bagheri, F.: A simplified sliding-mode control method for multi-level transformerless DVR. IET Power Electron. 15(8), 764–774 (2022)
14. Jeyaraj, K., Durairaj, D., Velusamy, A.I.S.: Development and performance analysis of PSO-optimized sliding mode controller-based dynamic voltage restorer for power quality enhancement. Int. Trans. Electr. Energy Syst. 30(3), 1–14 (2020)
15. Levant, A.: Sliding order and sliding accuracy in sliding mode control. Int. J. Control 58(6), 1247–1263 (1993)
16. Kamal, S., Chalanga, A., Moreno, J.A., Fridman, L., Bandyopadhyay, B.: Higher order super-twisting algorithm. In: Proceedings of IEEE Workshop on Applications of Computer Vision, pp. 1–5 (2014)
17. Chalanga, A., Kamal, S., Fridman, L.M., Bandyopadhyay, B., Moreno, J.A.: Implementation of super-twisting control: Super-twisting and higher order sliding-mode observer-based approaches. IEEE Trans. Ind. Electron. 63(6), 3677–3685 (2016)
18. Gonzalez, T., Member, S.: Variable gain super-twisting sliding mode control. IEEE Trans Automat Contr. 57(8), 2100–2105 (2012)
19. Utkin, V., Poznyak, A., Orlov, Y., Polyakov, A.: Conventional and high order sliding mode control. J. Franklin Inst. 357(15), (2020)
20. Feng, Y., Han, F., Yu, X.: Chattering free full-order sliding-mode control. Automatica 50(4), 1310–1314 (2014)
21. Hao, X., Luo, Y.: An SMC-ESO-based distortion voltage compensation strategy for PWM VSI of PMSM. IEEE J. Emerg. Sel. Top. Power Electron. 10(5), 5686–5697 (2022)
22. Zhao, Y., Dong, L.: Robust current and speed control of a permanent magnet synchronous motor using SMC and ADRC. Control Theory Technol. 17(2), 190–199 (2019)
23. Qu, L., Qiao, W., Qu, L.: An extended-state-observer-based sliding-mode speed control for permanent-magnet synchronous motors. IEEE J. Emerg. Sel. Top. Power Electron. 9(2), 1605–1613 (2021)
24. Qin, Q., Gao, G., Zhong, J.: Finite-time adaptive extended state observer-based dynamic sliding mode control for hybrid robots. IEEE Trans. Circuits Syst. II Express Briefs. 69(9), 3784–3788 (2022)
25. Wei, C., Xu, J., Chen, Q., Song, C., Qiao, W.: Full-order sliding-mode current control of permanent magnet synchronous generator with disturbance rejection. IEEE J. Emerg. Sel. Top. Power Electron. 4(1), 128–136 (2022)
26. Golestan, S., Freijedo, F.D., Vidal, A., Guerrero, J.M., Doval-Gandoy, J.: A quasi-type-1 phase-locked loop structure. IEEE Trans. Power Electron. 29(12), 6264–6270 (2014)
27. Kaura, V., Blasko, V.: Operation of a phase locked loop system under distorted utility conditions. IEEE Trans. Ind. Appl. 33(1), 58–63 (1997)
28. Ahmed, H., Biricik, S., Benbouzid, M.: Enhanced frequency adaptive demodulation technique for grid-connected converters. IEEE Trans. Ind. Electron. 68(11), 11053–11062 (2021)
29. Ahmed, H., Tir, Z., Verma, A.K., Ben Elghali, S., Benbouzid, M.: Quasi type-1 PLL with tunable phase detector for unbalanced and distorted three-phase grid. IEEE Trans. Energy Convers. 37(2), 1369–1378 (2022)
30. Sevilmiş, F., Karaca, H.: A fast hybrid PLL with an adaptive all-pass filter under abnormal grid conditions. Electr. Power Syst. Res. 184(3), 1 (2020)
31. Sevilmiş, F., Karaca, H.: Performance enhancement of DSOGI-PLL with a simple approach in grid-connected applications. Energy Rep. 8(1), 9–18 (2022)
32. Mellouli, M., Hamouda, M., Slama, J.B.H., Al-Haddad, K.: A third-order MAF based QT1-PLL that is robust against harmonically distorted grid voltage with frequency deviation. IEEE Trans. Energy Convers. 36(3), 1600–1613 (2021)
33. Gautam, S., Verma, A.K., Torres, M., Mandal, S., Taghizadeh, F., Akhtar, M.A.: Double demodulation type open-loop synchronization method for single-phase system. In: 2022 IEEE Global Conference on Computing, Power and Communication Technologies, GlobConPT 2022. Institute of Electrical and Electronics Engineers Inc. (2022)
34. Ahmed, H., Biricik, S., Komurcugil, H., Benbouzid, M.: Enhanced quasi type-1 PLL-based multi-functional control of single-phase dynamic voltage restorer. Appl. Sci. (Switzerland). 12(1), 146 (2022)
35. Verma, A.K., Burgos-Mellado, C., Gautam, S., Ahmed, H., Kim, T., Akhtar, M.A., et al.: Robust nonadaptive three-phase quasi-type-I PLL approach under distorted grid voltage conditions. In: 2022 IEEE Global Conference on Computing, Power and Communication Technologies, GlobConPT 2022 (2022)
36. Golestan, S., Monfared, M., Freijedo, F.D., Guerrero, J.M.: Dynamics assessment of advanced single-phase PLL structures. IEEE Trans. Ind. Electron. 60(6), 2167–2177 (2013)
37. Komurcugil, H., Bayhan, S., Guler, N., Biricik, S.: Super twisting sliding-mode control strategy for three-level dynamic voltage restorers. In: IEEE International Symposium on Industrial Electronics (2021)
38. Meng, Q., Hou, Z.: Active disturbance rejection based repetitive learning control with applications in power inverters. IEEE Trans. Control Syst. Technol. 29(5), 2038–2048 (2021)
39. Xu, Y., Zheng, B., Wang, G., Yan, H., Zou, J.: Current harmonic suppression in dual three-phase permanent magnet synchronous machine with extended state observer. IEEE Trans. Power Electron. 35(11), 12166–12180 (2020)
40. Pay, M.L., Cao, P., Sun, Y., McCluskey, D.: Luenberger observer based grid synchronization techniques for smart grid application. In: IECON Proceedings (Industrial Electronics Conference), pp. 4955–4960 (2020)

How to cite this article: Bagheri, F., Biricik, S., Ahmed, H., Komurcugil, H.: A second-order sliding mode control with active disturbance rejection for dynamic voltage restorers. IET Power Electron. 1–12 (2023). https://doi.org/10.1049/pel2.12490